Title

Improved Synthesis of Chiral Pyrrolidine Inhibitors and Their Binding Properties to Neuronal Nitric Oxide Synthase

Journal

Journal of Medicinal Chemistry, 54(18)

ISSN

0022-2623

Authors

Xue, Fengtian
Kraus, James M
Labby, Kristin Jansen
et al.

Publication Date

2011-09-22

DOI

10.1021/jm200411j

Published in final edited form as:
J Med Chem. 2011 September 22; 54(18): 6399–6403. doi:10.1021/jm200411j.

Improved Synthesis of Chiral Pyrrolidine Inhibitors and Their Binding Properties to Neuronal Nitric Oxide Synthase

Fengtian Xue[1,§,†], **James M. Kraus**[1,§], **Kristin Jansen Labby**[1], **Haitao Ji**[1], **Jan Mataka**[1], **Guoyao Xia**[1], **Huiying Li**[2], **Silvia L. Delker**[2], **Linda J. Roman**[3], **Pavel Martásek**[3,4], **Thomas L. Poulos**[2,*], and **Richard B. Silverman**[1,*]

[1]Department of Chemistry, Department of Molecular Biosciences, Chemistry of Life Processes Institute, Center for Molecular Innovation and Drug Discovery, Northwestern University, 2145 Sheridan Road, Evanston, Illinois 60208-3113, USA

[2]Departments of Molecular Biology and Biochemistry, Pharmaceutical Chemistry, and Chemistry, University of California, Irvine, California 92697-3900

[3]Department of Biochemistry, The University of Texas Health Science Center, San Antonio, Texas 78384-7760

[4]Department of Pediatrics and Center for Applied Genomics, 1st School of Medicine, Charles University, Prague, Czech Republic

Abstract

We report an efficient synthetic route to chiral pyrrolidine inhibitors of neuronal nitric oxide synthase (nNOS) and crystal structures of the inhibitors bound to nNOS and to endothelial NOS. The new route enables versatile structure activity relationship studies on the pyrrolidine-based scaffold, which can be beneficial for further development of nNOS inhibitors. The X-ray crystal structures of three new fluorine-containing inhibitors bound to nNOS provide insights into the effect of the fluorine atoms on binding.

INTRODUCTION

Selective inhibition of neuronal nitric oxide synthase (nNOS) over its closely related isozymes, inducible nitric oxide synthase (iNOS) and endothelial nitric oxide synthase (eNOS), has attracted tremendous drug discovery efforts for neurotoxicity and certain neurodegenerative conditions such as Parkinson's, Alzheimer's, Huntington's diseases, and cerebral palsy.[1–5] As part of our research program directed toward developing novel nNOS inhibitors, we recently disclosed a series of *gem*-difluorinated monocationic inhibitors including compounds **1a** and **1b**, which are potent and highly selective inhibitors of nNOS.[6,7] Moreover, according to the results of detailed pharmacokinetic studies,[7,8]

*Correspondence to Prof. Richard B. Silverman at the Department of Chemistry, Agman@chem.northwestern.edu; 847-491-5653. Prof. Thomas L. Poulos, poulos@uci.edu; 949-824-7020.
§These authors shared equally in their contributions to this paper.
†Present Address: Department of Pharmaceutical Sciences, University of Maryland School of Pharmacy, 20 N. Pine Street, Room N719, Baltimore, Maryland, 21201, USA

¶The PDB codes for Figure 1 are as follows: nNOS-**8a**: 3PNE; nNOS-**8b**: 3PNF; nNOS-**8c**: 3PNG; eNOS-**8c**: 3PNH; nNOS-**8d**: 3SVP; nNOS-**8e**: 3SVQ.

SUPPORTING INFORMATION AVAILABLE: Detailed procedure for the syntheses of compounds **12**, **13**, 1**4**, **15a–b**, **9**, **16**, **17**, **18,** and **19a–e**, enzyme assays of **8a–e**, and crystal structures of **8a–e** in the active site of enzyme are available free of charge via the Internet at http://pubs.acs.org.

compound **1b** has demonstrated intriguing cell membrane permeability and oral bioavailability, which makes it a promising drug candidate for neurodegenerative diseases.

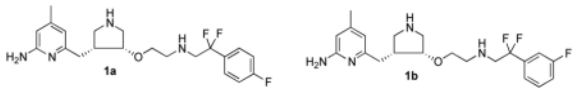

Although they possess desirable potency, selectivity, and pharmacokinetic properties, it is difficult to prepare gram-scale quantities of **1b** for a comprehensive preclinical study.[7,8] The previously reported route takes 16 steps starting from 4,6-dimethyl-2-aminopyridine (Scheme 1). Several of the steps suffered from unsatisfactory yields, resulting in an overall yield of less than 1%.[7,8] In particular, the late stage benzyl deprotection step, employing a high temperature catalytic hydrogenation of the *N*-Boc-*N*-benzyl-protected intermediate **2**, proceeded poorly to give **3**. As a result, the utility of this route was dramatically compromised by the present lack of scalability. More importantly, the strong reducing conditions used to remove the benzyl protecting group prohibited the possibility of incorporating reduction sensitive functional groups (e.g., nitriles, ketones, alkenes, and halophenyls) into the inhibitors, which significantly impaired structure-activity optimization based on this scaffold. For instance, attempts to remove the benzyl protecting group of **4** led to dechlorination (**5**, Scheme 2). Removal of the benzyl protecting group of **6** by catalytic hydrogenation led to a partial reduction of the cyclopropyl ring in **7**.[9]

We report here a synthesis with improved overall yield and functional group compatibility. In the current method, the problematic benzyl protecting group in the previous synthesis is replaced by a Boc-protecting group. The new route not only produces **1b** in an enhanced overall yield, but also provides a way to synthesize inhibitors with reduction-sensitive chlorophenyl groups.

CHEMISTRY

As shown in Scheme 3, the synthesis of key precursor **9** began with Boc-protected 4,6-dimethylaminopyridine **10**. Compound **10** was treated with two equivalents of *n*-butyllithium (*n*-BuLi), and the resulting dianion was allowed to react with *tert*-butyl 6-oxa-3-azabicyclo[3.1.0]hexane-3- carboxylate[6] to generate the *trans*-alcohol (**11**) in modest yields. Attempts to convert **11** directly to **14** failed because the free hydroxyl group of **11** is more reactive toward $(Boc)_2O$ than the carbamate NH group, and the hydrolytic stability of the formed carbonate is very similar to that of the di-Boc-protected aminopyridine. Therefore, we had to use a three-step procedure to convert **11** to **14**. Di-Boc protection of **10** also was fruitless because one of the Boc groups is transferred to the oxyanion of **11** upon condensation of di-Boc-**9** with *tert*-butyl 6-oxa-3-azabicyclo[3.1.0]hexane-3-carboxylate, as described earlier.[10a] The hydroxyl group of **11** was first protected with *t*-butyldimethylsilyl chloride (TBSCl) in the presence of imidazole to give the silyl ether (**12**) in excellent yields. Next, the NH of the carbamate group on the pyridine ring was further protected with another Boc protecting group using $(Boc)_2O$ in the presence of 4-dimethylaminopyridine (DMAP) to yield **13** in high yields, then the silyl ether was cleaved using tetrabutylammonium fluoride (TBAF) to provide the tri-Boc protected alcohol (**14**) in very high yields. Finally, the two enantiomers of **14** were resolved through their camphanic ester derivatives (**15a** and **15b**) employing a Mitsunobu reaction using (*S*)-(−)-camphanic acid as the nucleophile. The ester linkage of **15b** was hydrolyzed carefully using Na_2CO_3 in $MeOH/H_2O$ to provide chiral precursor **9** in excellent yields.

Allylation of chiral *cis*-alcohol **9** in the presence of allyl methyl carbonate using $Pd(PPh_3)_4$ as a catalyst provided **16** in good yields (Scheme 4).[10–11] Alkene **16** was treated with ozone,

followed by dimethyl sulfide to generate **17** in excellent yields. Aldehyde **17** underwent a reductive amination reaction with the corresponding amines in the presence of $NaHB(OAc)_3$ to give **18, 19a–e** in high yields. Finally, the three Boc-protecting groups were removed simultaneously in HCl to provide the final inhibitors in excellent yields.

RESULTS AND DISCUSSION

We have determined the crystal structures of rat nNOS with inhibitors **8a–e** bound and that of bovine eNOS in complex with **8c**. The pdb codes are given in Supporting Information Table 1. As expected from the chirality of their pyrrolidine moiety, inhibitors **8a–e** adopt the same flipped binding mode as lead compound **1a–b** (Figure 1).[7] The aminopyridine motif extends to the surface hydrophobic pocket (Tyr706, Leu337, and Met336) in nNOS, forming a charge-charge interaction with the heme propionate D, and a π–π stacking interaction with the aromatic side chain of Tyr706 in its newly adapted conformation. Substitution of the *m*-fluoro atom in the phenyl tail of **1b** with a larger chlorine atom slightly increases the potency (1.3-fold) of the inhibitor (**8a** vs **1b**, Table 1). A comparison between the structures of nNOS-**8a** (Fig. 1A) and nNOS-**1b** provides some clues as to why nNOS prefers the *m*-chloro over *m*-fluoro atom on the phenyl group. Similar to what was observed for nNOS-**1b**[7] the 2,2-difluoro-2-(*m*-chlorophenyl)ethyl moiety of **8a** has adopted two conformations, with the CF_2 group pointing both away from (major) and toward (minor) the heme. Residual Fo-Fc difference density is present especially around the fluorine atoms if only one conformation is modeled clearly, indicating two conformations. The two different conformations also result in two slightly different orientations of the chlorophenyl group, which is consistent with two conformations. However, because of the bulkier chlorine atom in **8a** there is increased Van der Waals contact and the phenyl ring has been pushed closer to the Glu592 side chain, but is still well tolerated. The Glu592 side chain shows two rotamers in the nNOS-**8a** structure, which were seen in nNOS-**1b** as well. The new Glu592 rotamer forms a new hydrogen bond to the amino nitrogen of the inhibitor (Fig. 1A). The active site of eNOS might alsoaccommodate the *m*-chlorophenyl ring better; therefore, the selectivity of **8a** for nNOS over eNOS has dropped 20-fold, which makes this inhibitor comparable to inhibitor **1a**.

Inhibitor **8b**, the corresponding *o*-chloro isomer of compound **8a**, has 2-fold lower potency for rat nNOS (**8b** vs **8a**, Table 1). However, eNOS does not show a preference for inhibitors **8b** and **8a**. The structure of nNOS-**8b** (Fig. 1B) reveals only one conformation for the inhibitor where the CF_2 group points toward the heme. In this conformation one of the fluorine atoms makes an unfavorable intramolecular contact with the chlorine atom on the phenyl ring. However, there is no electron density indicating an altered orientation for the CF_2 group that avoids this unfavorable contact. This steric hindrance may partially account for the 2-fold drop in potency for **8b** compared to **8a**. When both *meta* positions of the phenyl ring are substituted (**8d**), the conformation of the phenyl ring is determined by the bulkier chlorine atom and the conformation is more like **8a** than **1b**. This ring is still well tolerated in the active site, and, of the CF_2 analogs reported here (**1a–b, 8a–b, 8d–e**), **8d** is the most potent of the series. Interestingly, the side chain of **8d** shows only one conformation because the *meta* disubstituted ring is too large to be accommodated in the alternate conformation. Inhibitor **8e** is the least potent analog of the series. Similar to **8b**, *ortho* substitution in **8e** leads to an intramolecular clash between fluorine of the ring and the CF_2 group, and again, only one side chain conformation is observed with CF_2 pointing downward to the heme (Figures 1B and 1F).

Inhibitor **8c**, a mixture of diastereomers, is the monofluoro methylene derivative of **1b** with a chiral pyrrolidine core. The mixture shows increased potency for rat nNOS (**8c** vs **1b**, Table 1). This may result from the higher basicity of the amino group in the lipophilic tail of

8c compared to that of **1b**.[8] However, the nNOS selectivity of **8c** over eNOS is somewhat diminished compared with that for **1b** because of its relatively higher potency toward eNOS. The structures of **8c** bound to both nNOS and eNOS were obtained (Fig. 1C and 1D). In both structures, the same binding mode for **8c** is observed, with its single fluorine atom pointing down toward the heme. Apparently, despite being a mixture of diastereomers, the (*R*,*R*,*R*)-diastereomer has greater binding affinity to the isozymes than the (*R*,*R*,*S*)-diastereomer because the observed electron density for the fluorine atom only supports one position (*R*). This may be because there is no unfavorable contact between this fluorine atom and heme propionate A in contrast to the clashes observed for the CF_2 group in its "downward" conformation in the nNOS-**8a** structure (Fig. 1A). The amino group in the lipophilic tail of the inhibitor lures Glu592 of nNOS (Glu363 of eNOS) into an alternate rotamer by hydrogen bonding.

Structure activity relationship (SAR) studies demonstrate the key role of the *meta* substituent in **1b**, **8c**, and **8d** for retaining high inhibitory activity for rat nNOS. A bulkier *m*-chloro group in **8a** increases potency relative to the *m*-fluoro substituent, but leads to a loss in selectivity over the other two isoforms. Although *m*-chloro and *m*-fluoro disubstitution (**8d**) achieves another small boost in potency, it also results in an additional drop in selectivity. The *o*-chloro group in **8b** or *o*-fluoro group in **8e** leads to tight intramolecular contacts with its CF_2 group, which is accompanied by an unfavorable side chain conformation and a drop in potency. The *p*-fluoro in **1a** forces its CF_2 group into a downward conformation, weakening the hydrogen bond from the amino group to the Glu592 side chain. It seems then, that only *meta* substituents place the phenyl ring in the right position to optimize van der Waals contact with the hydrophobic pocket surrounded by Val567 and Phe584 in nNOS,[7] and *m*-fluoro inhibitor **1b** achieves the optimum balance between potency and selectivity.

CONCLUSION

In summary, an improved synthesis of chiral pyrrolidine inhibitors of nNOS has been developed. Compared with the reported synthesis, it is three steps shorter with an overall yield of approximately 10% (>10-fold larger). It also enables expanded SAR studies on the pyrrolidine-based scaffold, which can be beneficial for further development of nNOS inhibitors.

EXPERIMENTAL SECTION

The purity of the final compounds was determined by HPLC analysis to be ≥95%. For experimental details, see the Supporting Information.

6-(((3*R*,4*R*)-4-(2-((2,2-Difluoro-2-(3-fluorophenyl)ethyl)amino)ethoxy)pyrrolidin-3-yl)methyl)-4-methylpyridin-2-amine (1b)

To a solution of **18a** (60 mg, 85 umol) in MeOH (2 mL) was added 6 N HCl (4 mL) at room temperature. The mixture was stirred for 12 h and then concentrated. The crude product was purified by recrystallization ($EtOH/H_2O$) to give inhibitor **1b** (40 mg, 99%) as a tri-HCl salt; $[\alpha]^{20}$ +6.25 (*c* 4, MeOH).

6-(((3*R*,4*R*)-4-(2-((2,2-Difluoro-2-(3-chlorophenyl)ethyl)amino)ethoxy)pyrrolidin-3-yl)methyl)-4-methylpyridin-2-amine (8a)

To a solution of **18b** (70 mg, 0.10 mmol) in MeOH (2 mL) was added 6 N HCl (4 mL) at room temperature. The mixture was stirred for 12 h and then concentrated. The crude product was purified by recrystallization ($EtOH/H_2O$) to give inhibitor **8a** (50 mg, 95%) as a tri-HCl salt: ^1H NMR (500 MHz, D_2O) δ 2.19 (s, 3H), 2.60–2.75 (m, 1H), 2.85–2.95 (m,

1H), 3.00–3.10 (m, 2H), 3.20–3.30 (m, 1H), 3.30–3.45 (m, 3H), 3.55–3.60 (d, *J* = 13.0 Hz, 1H), 3.65–3.70 (m, 1H), 3.75–3.90 (m, 3H), 4.15 (d, *J* = 3.0 Hz, 1H), 6.41 (s, 1H), 6.55 (s, 1H), 7.30–7.45 (m, 3H), 7.52 (s, 1H); ^{13}C NMR (125 MHz, D_2O) δ 20.0, 29.2, 41.3, 41.4, 47.0, 47.4, 49.1, 51.7, 63.6, 78.3, 110.4, 114.0, 118.2, 123.39, 123.42, 123.47, 125.07, 125.12, 130.7, 131.5, 133.9, 134.4, 145.4, 153.9, 158.1; LC-TOF ($M+H^+$) calcd for $C_{21}H_{28}ClF_2N_4O$ 425.1920, found 425.1919.

6-(((3*R*,4*R*)-4-(2-((2,2-Difluoro-2-(2-chlorophenyl)ethyl)amino)ethoxy)pyrrolidin-3-yl)methyl)-4-methylpyridin-2-amine (8b)

Inhibitor **8b** was synthesized using a similar procedure to that for **8a** (50 mg, 95%) as a tri-HCl salt: ^{1}H NMR (500 MHz, D_2O) δ 2.19 (s, 3H), 2.60–2.75 (m, 1H), 2.85–2.95 (m, 1H), 3.03–3.08 (t, *J* = 11.5 Hz, 1H), 3.19 (s, 1H), 3.21–3.25 (dd, *J* = 3.0, 13.0 Hz, 1H), 3.35–3.42 (m, 3H), 3.52–3.58 (d, *J* = 13.0 Hz, 1H), 3.63–3.66 (m, 1H), 3.82–3.88 (m, 1H), 3.90–4.00 (m, 2H), 4.14–4.16 (t, *J* = 3.5 Hz, 1H), 6.42 (s, 1H), 6.54 (s, 1H), 7.30–7.35 (m, 1H), 7.40–7.45 (m, 2H), 7.55–7.60 (m, 1H); ^{13}C NMR (125 MHz, D_2O) δ 21.0, 29.0, 41.2, 47.0, 47.4, 48.8, 49.2, 50.3, 50.5, 63.4, 78.2, 110.4, 113.9, 118.1, 127.57, 127.63, 127.70, 129.1, 130.8, 131.4, 131.5, 133.1, 145.5, 153.9, 158.1; LC-TOF ($M+H^+$) calcd for $C_{21}H_{28}ClF_2N_4O$ 425.1920, found 425.1919.

6-(((3*R*,4*R*)-4-(2-((2-fluoro-2-(3-fluorophenyl)ethyl)amino)ethoxy)pyrrolidin-3-yl)methyl)-4-methylpyridin-2-amine (8c)

Inhibitor **8c** was synthesized as a mixture of two diastereomers using a similar procedure to that for **8a** (32 mg, 90%) as a tri-HCl salt: ^{1}H NMR (500 MHz, D_2O) δ 2.19 (s, 3H), 2.65–2.75 (m, 1H), 2.85–2.95 (m, 1H), 3.03–3.11 (m, 1H), 3.20 (s, 1H), 3.21–3.25 (dd, *J* = 3.0, 13.0 Hz, 1H), 3.30–3.45 (m, 4H), 3.50–3.58 (m, 2H), 3.60–3.66 (m, 1H), 3.80–3.85 (m, 1H), 4.14–4.16 (m, 1H), 5.80–6.00 (m, 1H), 6.46 (s, 1H), 6.50–6.55 (m, 1H), 7.00–7.15 (m, 3H), 7.30–7.41 (m, 1H); ^{13}C NMR (125 MHz, D_2O) δ 21.0, 29.0, 29.1, 41.3, 41.4, 43.7, 43.9, 47.0, 47.1, 47.3, 48.7, 49.2, 49.3, 51.3, 51.5, 51.7, 51.8, 63.6, 63.9, 78.2, 88.4, 89.8, 110.4, 112.48, 112.54, 112.56, 112.61, 112.69, 112.72, 112.74, 114.0, 114.1, 116.3, 116.5, 116.6, 121.35, 121.40, 121.46, 121.49, 121.51, 130.85, 130.92, 131.0, 136.8, 136.99, 137.02, 145.60, 145.64, 153.85, 153.86, 158.11, 158.12, 161.6, 163.5; LC-TOF ($M+H^+$) calcd for $C_{21}H_{29}F_2N_4O$ 391.2309, found 391.2288.

6-(((3*R*,4*R*)-4-(2-((2,2-Difluoro-2-(3-chloro-5-fluorophenyl)ethyl)amino)ethoxy)pyrrolidin-3-yl)methyl)-4-methylpyridin-2-amine (8d)

Inhibitor **8d** was synthesized as a mixture of two diastereomers using a similar procedure to that for **8a** (7 mg, 80%) as a tri-HCl salt: ^{1}H NMR (500 MHz, MeOD) δ 2.35 (s, 3H), 2.80–2.87 (m, 1H), 2.93–2.98 (m, 1H), 3.07–3.13 (m, 1H), 3.23–3.27 (m, 1H), 3.38–3.45 (m, 1H), 3.51–3.56 (m, 2H), 3.50–3.58 (m, 2H), 3.65–3.68 (d, *J* = 13.0 Hz, 1H), 3.73–3.79 (m, 2H), 3.94–3.99 (m, 1H), 4.00–4.07 (m, 1H), 4.19–4.21 (m, 1H), 6.66 (s, 1H), 6.67 (s, 1H), 7.42–7.46 (m, 2H), 7.56 (s, 1H); ^{13}C NMR (125 MHz, MeOD) δ 22.0, 30.4, 43.5, 52.5, 52.7, 64.9, 80.0, 111.5, 112.8, 112.9, 115.1, 120.2, 120.4, 123.1, 137.47, 137.48, 147.95, 156.0, 159.2, 163.2, 165.2; LC-TOF ($M+H^+$) calcd for $C_{21}H_{26}ClF_3N_4O$ 443.1747, found 443.3306.

6-(((3*R*,4*R*)-4-(2-((2,2-Difluoro-2-(2,3-difluorophenyl)ethyl)amino)ethoxy)pyrrolidin-3-yl)methyl)-4-methylpyridin-2-amine (8e)

Inhibitor **8e** was synthesized as a mixture of two diastereomers using a similar procedure to that for **8a** (12 mg, 75%) as a tri-HCl salt: ^{1}H NMR (500 MHz, MeOD) δ 2.35 (s, 3H), 2.82–2.88 (m, 1H), 2.95–3.00 (m, 1H), 3.08–3.14 (m, 1H), 3.23–3.30 (m, 1H), 3.40–3.44 (m, 1H), 3.53–3.55 (m, 2H), 3.60 (d, *J* = 13 Hz, 1H), 3.77–3.79 (m, 1H), 3.95–3.97 (m, 1H), 4.04–4.10 (m, 2H), 4.19–4.20 (m, 1H), 6.66 (s, 1H), 6.67 (s, 1H), 7.32–7.55 (m, 3H); ^{13}C NMR

(125 MHz, MeOD) δ 22.0, 30.35, 30.40, 43.5, 49.9, 50.4, 52.5, 65.0, 79.9, 111.5, 115.1, 122.2, 122.3, 123.5, 126.7, 137.47, 137.48, 147.9, 148.0, 156.0, 159.2; LC-TOF ($M+H^+$) calcd for $C_{21}H_{26}F_4N_4O$ 427.2043, found 427.4021.

Supplementary Material

Refer to Web version on PubMed Central for supplementary material.

Acknowledgments

We are grateful to the National Institutes of Health, Grants GM049725 to RBS, GM057353 to TLP, and GM052419 to Dr. Bettie Sue Siler Masters, with whose lab PM and LJR are affiliated, and Grant No. AQ1192 from The Robert A. Welch Foundation to BSSM. BSSM also is grateful to the Welch Foundation for a Robert A. Welch Foundation Distinguished Professorship in Chemistry (AQ0012). P.M. is supported by grants 0021620806 and 1M0520 from MSMT of the Czech Republic for financial support of this research. We thank the SSRL beamline staff for their support during remote X-ray diffraction data collection.

Abbreviations

nNOS	neuronal nitric oxide synthase
NO	nitric oxide
eNOS	endothelial nitric oxide synthase
iNOS	inducible nitric oxide synthase
***n*-BuLi**	*n*-butyllithium
TBSCl	*t*-butyldimethylsilyl chloride
DMAP	4-dimethylaminopyridine
TBAF	tetrabutylammonium fluoride
SAR	structure activity relationship

References

1. Zhang L, Dawson VL, Dawson TM. Role of nitric oxide in Parkinson’s disease. Pharmacol Ther. 2006; 109:33–41. [PubMed: 16005074]
2. Dorheim MA, Tracey WR, Pollock JS, Grammas P. Nitric oxide synthase activity is elevated in brain microvessels in Alzheimer’s Disease. Biochem Biophys Res Commun. 1994; 205:659–665. [PubMed: 7528015]
3. Norris PJ, Waldvogel HJ, Faull RLM, Love DR, Emson PC. Decreased neuronal nitric oxide synthase messenger RNA and somatostatin messenger RNA in the striatum of Huntington’s disease. Neuroscience. 1996; 72:1037–1047. [PubMed: 8735228]
4. Ji H, Tan S, Igarashi J, Li H, Derrick M, Martásek P, Roman LJ, Vásquez-Vivar J, Poulos TL, Silverman RB. Selective neuronal nitric oxide synthase inhibitors for prevention of cerebral palsy. Ann Neurol. 2009; 65:209–217. [PubMed: 19235180]
5. Ji, H.; Erdal, EP.; Litzinger, EA.; Seo, J.; Zhu, Y.; Xue, F.; Fang, J.; Huang, J.; Silverman, RB. Selective neuronal nitric oxide synthase inhibitors frontiers in medicinal chemistry. Reitz, AB.; Choudhary, MI.; Atta-ur-Rahman, editors. Vol. 4. Bentham Science Publishers; 2009. p. 842-882.volume 5
6. Lawton GR, Ranaivo HR, Wing LK, Ji H, Xue F, Martesek P, Roman LJ, Watterson DM, Silverman RB. Analogues of 2-aminopyridine-based selective inhibitors of neuronal nitric oxide synthase with increased bioavailability. Bioorg Med Chem. 2009; 17:2371–2380. [PubMed: 19268602]

7. Xue F, Li H, Delker S, Fang J, Martásek P, Roman LJ, Poulos TL, Silverman RB. Potent, highly selective, and orally bioavailable *gem*-difluorinated monocationic inhibitors of neuronal nitric oxide synthase. J Am Chem Soc. 2010; 132:14229–14238. [PubMed: 20843082]

8. Xue F, Fang J, Lewis WW, Martasek P, Roman LJ, Silverman RB. Potent and selective neuronal nitric oxide synthase inhibitors with improved cellular permeability. Bioorg Med Chem Lett. 2010; 20:554–557. [PubMed: 19963381]

9. Xue F, Li H, Kraus JM, Ji H, Mataka J, Labby KJ, Poulos TL, Silverman RB. unpublished results.

10. Xue F, Silverman RB. An alkoxide anion triggered tert-butyloxycarbonyl group migration. Mechanism and application. Tetrahedron Lett. 2010; 51:2536–2538. [PubMed: 20414457]

11. Haight AR, Stoner EJ, Peterson MJ, Grover VK. General method for the palladium-catalyzed allylation of aliphatic alcohols. J Org Chem. 2003; 68:8092–8096. [PubMed: 14535788]

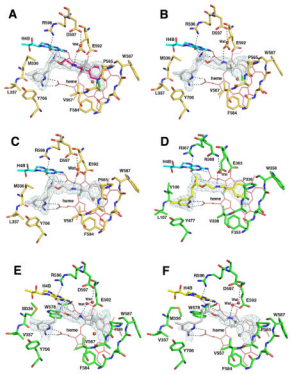

Figure 1.

The active site structures in enzyme-inhibitor complexes: (A) nNOS-**8a**, (B) nNOS-**8b**, (C) nNOS-**8c**, (D) eNOS-**8c,** (E) nNOS-**8d**, and (F) nNOS-**8e**. The sigmaA weighted 2Fo – Fc electron density map for each bound inhibitor at 1σ contour level is shown for panels A to D and the omit Fo – Fc density map at 2.5 σ contour level shown for panels E and F. Major hydrogen bonds are drawn with dashed lines. Alternate side chain rotamers are observed for Glu592 in nNOS or Glu363 in eNOS in panels A to D. The inhibitor **8a** also shows two conformations in its lipophilic tail (colored as gray and magenta in panel A). The density for part of inhibitor **8e** is weak as shown, but the model presented in panel F is supported by the 2Fo – Fc map at lowered contour level (0.5 σ). Figures were prepared with PyMol (www.pymol.org). The PDB codes are as follows: nNOS-**8a**: 3PNE; nNOS-**8b**: 3PNF; nNOS- **8c**: 3PNG; eNOS-**8c**: 3PNH; nNOS-**8d**: 3SVP; nNOS-**8e**: 3SVQ.

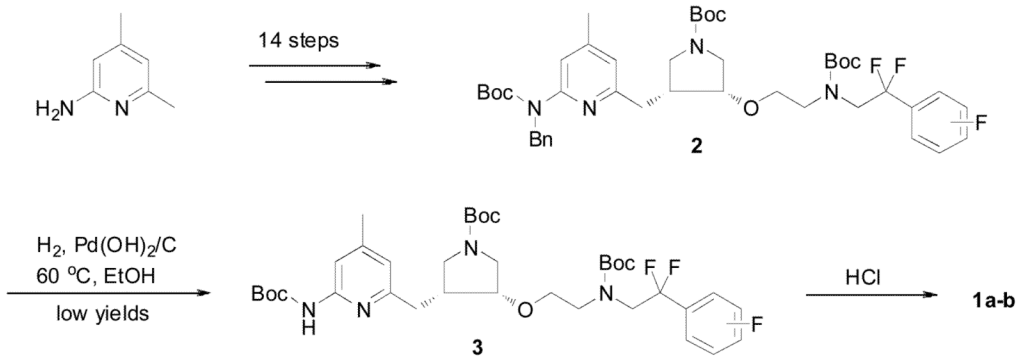

Scheme 1.
Previous Synthetic Route to 1a–b.

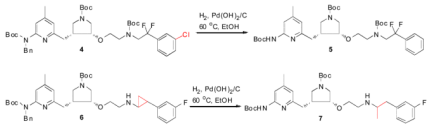

Scheme 2.

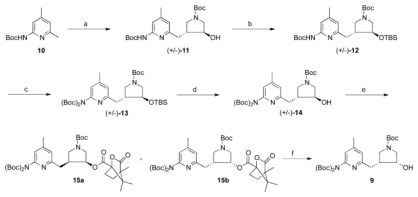

Scheme 3. Synthesis of 9.[a]

[a] Reagents and conditions: (a) (i) *n*-BuLi (2eq.), −78 °C to rt, (ii) epoxide, −78 °C to rt, 41%; (b) TBSCl, imidazole, DMF, rt, 30 h, 93%; (c) $(Boc)_2O$, DMAP, rt, 24 h, 95%; (d) TBAF, rt, 15 min, 99%; (e) (*S*)-(−)-camphanic acid, DIAD, rt, 16 h, 94%; (f) Na_2CO_3, H_2O/MeOH, 35 °C, 30 min, 97%.

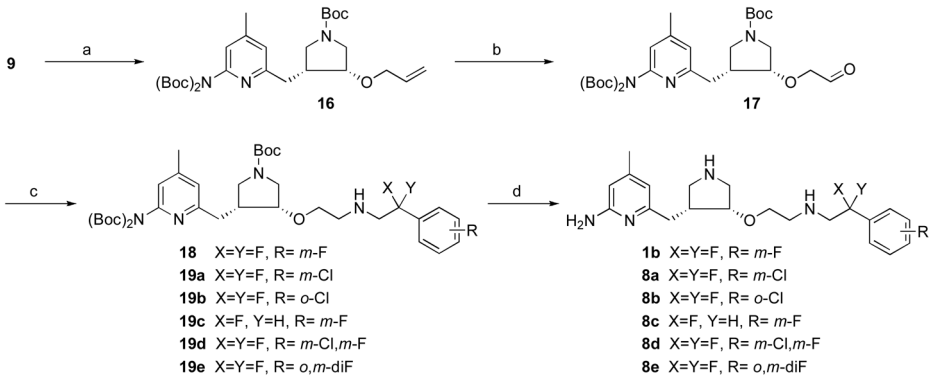

Scheme 4. Synthesis of 1b and 8a–e.[a]

[a] Reagents and conditions: (a) allyl methyl carbonate, $Pd(PPh_3)_4$, 45 °C, 5 h, 66%; (b) O_3, −78 °C, 30 min, (ii) Me_2S, −78 °C to rt, 2 h, 87%; (c) amine hydrochloride, triethylamine, $NaHB(OAc)_3$, rt, 3 h, 86–91%; (d) 6 N HCl in MeOH (2:1), rt, 12 h, 90–99%.

Table 1

K_i Values of Inhibitors for Rat nNOS, Bovine eNOS and Murine iNOS[a]

Compound	nNOS (μM)	eNOS (μM)	iNOS (μM)	selectivity[b]	
				n/e	n/i
1a	0.16	31	190	194	1188
1b[c]	0.11	130	25	1182	227
8a	0.086	16	78	186	907
8b	0.17	27	91	159	535
8c	0.026	19	26	731	1000
8d	0.077	17	17	221	221
8e	0.18	49	130	272	722

[a] The K_i values were calculated based on the directly measured IC_{50} values, which represent at least duplicate measurements with standard deviations of ±10%. There is high homology among these isozymes from different species.[5]

[b] The ratio of K_i (eNOS or iNOS) to K_i (nNOS).

[c] The K_i (nNOS) for inhibitor **1b** is different from that previously reported because of the use of a new high throughput assay improving both speed and reproducibility.